Eur. Phys. J. Plus (2022) 137:396
https://doi.org/10.1140/epjp/s13360-022-02606-w

THE EUROPEAN PHYSICAL JOURNAL PLUS

Regular Article

Impact of loss mechanisms through defects on $Sb_2(S_{1-x}Se_x)_3$/CdS solar cells with p-n structure

Maykel Courel[1,a], Thalía Jimenez[2], I. Montoya De Los Santos[3], J. P. Morán-Lázaro[1], M. Ojeda Martinez[1], L. M. Pérez[4], D. Laroze[5], E. Feddi[6], F. J. Sánchez-Rodríguez[7]

[1] Centro Universitario de los Valles (CUValles), Universidad de Guadalajara, Carretera Guadalajara - Ameca Km. 45.5, 46600 Ameca, Jalisco, Mexico
[2] Centro de Investigaciones en Ingeniería Y Ciencias Aplicadas, Universidad Autónoma del Estado de Morelos, 62209 Cuernavaca, Morelos, Mexico
[3] Instituto de Estudios de La Energía, Universidad del Istmo, 70760 Santo Domingo Tehuantepec, Oaxaca, Mexico
[4] Departamento de Física, FACI, Universidad de Tarapacá, Casilla 7D, Arica, Chile
[5] Instituto de Alta Investigación, CEDENNA, Universidad de Tarapacá, Casilla 7D, Arica, Chile
[6] Group of Optoelectronic of Semiconductors and Nanomaterials, ENSAM, Mohammed V University in Rabat, Rabat, Morocco
[7] Facultad de Ciencias Físico-Matemáticas, Universidad Autónoma de Sinaloa, 80010 Culiacán, Sinaloa, Mexico

Received: 10 October 2021 / Accepted: 15 March 2022
© The Author(s), under exclusive licence to Società Italiana di Fisica and Springer-Verlag GmbH Germany, part of Springer Nature 2022

Abstract Antimony sulfide selenide ($Sb_2(S_{1-x}Se_x)_3$) material has emerged as a potential candidate for solar cell fabrication. However, up-to-date, efficiencies of about 7% have been widely reported for solar cells based on this absorber material under a p–n junction. Further experimental and theoretical attempts are required to find the main limitations of this type of solar cell. In this work, a theoretical study is presented to evaluate the influence of loss mechanisms on antimony sulfide selenide solar cells. In particular, the effect of bulk recombination, tunneling enhanced recombination and $Sb_2(S_{1-x}Se_x)_3$/CdS interface recombination on device parameters is evaluated at different $Sb_2(S_{1-x}Se_x)_3$ compositions. Bulk and interface defects were identified as the main loss mechanisms degrading device efficiency, while the effect of electric field in enhancing carrier recombination in the depletion region can be neglected. In addition, it is demonstrated that a further efficiency increase over 14% could be only obtained for an electron lifetime higher than 100 ns and a recombination speed shorter than 1 cm/s at the $Sb_2(S_{1-x}Se_x)_3$/CdS interface.

1 Introduction

The thin film solar cell technology is mainly based on CdTe and CIGS semiconductors. In particular, efficiencies higher than 20% have been reported for solar cells based on these compounds [1]. However, the low abundance of In, Te, and Ga along with Cd toxicity are important drawbacks for the massive production. As a result, other absorber materials have been proposed and studied for solar cell fabrication. Recently, antimony sulfide selenide ($Sb_2(S_{1-x}Se_x)_3$) semiconductor has been intensively studied by the scientific community working on thin film solar cells, since it presents direct optical transitions resulting in a high absorption coefficient ($>10^4$ cm^{-1}), a p-type conductivity, and an optimal band-gap for photovoltaic applications [2–4]. In particular, band-gap values in the range of 1.08–1.62 eV can be obtained for Se/(S + Se) compositional ratios between 1 and 0, covering nearly the whole solar spectrum [5]. Besides, unlike CdTe and CIGS, constituent elements of $Sb_2(S_{1-x}Se_x)_3$ compound are low toxic and abundant in the earth's crust. In addition, when comparing antimony sulfide selenide semiconductor with other emerging absorber materials such as kesterite family consisting of at least four elements, secondary phases are less likely to be form in the former. Furthermore, while temperatures higher than 500 °C are often used in kesterite technology for crystallization [6], lower temperatures are needed for antimony sulfide selenide processing. In fact, temperatures shorter than 400 °C are often reported for antimony sulfide selenide thin film deposition [7]. In general, all of these mentioned points make this compound attractive for photovoltaic applications.

The antimony sulfide selenide compound has been processed by some chemical and physical routes [3, 7]. However, its application to photovoltaic is in an early stage, with an increased number of publications each year, which is still lower than the number found for other technologies such as kesterites or perovskites. So far, most antimony sulfide selenide cells in p–n junction have shown efficiency values lower than 7% under planar geometry [8], with the exception of a n-i-p structure proposal, which was able to achieve a maximum efficiency of 10% [4]. Nevertheless, these values are shorter than the maximum expected for this technology (29%) [9]. In order to increase antimony sulfide selenide device efficiency, more experimental and theoretical works focused on finding the limiting factors are mandatory. In particular, the mechanisms behind low solar cell behavior are still unclear. So far, there is scant information on dominant loss mechanisms in this technology. It is known that modeling and simulation works favor a better understanding of mechanisms limiting solar cell efficiency and thereby provide possible routes for device promotion. In particular, analytical approaches are very useful to understand the physics governing the transport mechanism in devices. In a previous work,

[a] e-mail: maykel.courel@academicos.udg.mx (corresponding author)

Published online: 28 March 2022

it was demonstrated that defects in general can reduce device efficiency to 7% [9]. However, the defects nature—bulk or interface defects—was not studied in detail. Bulk and absorber/buffer interface defects are often identified as dominant in photovoltaic technology [10]. In particular, carrier recombination due to defects could be increased with the assistance of the electrical potential created at the device junction, through tunneling mechanisms (tunneling enhanced recombination) [11]. In a recent experimental work, the loss mechanisms influence on Sb_2Se_3 solar cells was studied, where defects at Sb_2Se_3/CdS interface were shown as likely to be dominant in this technology [12]. Therefore, more attention should be paid to understanding the role that is playing defects at antimony sulfide selenide bulk and absorber/CdS interface for achieving higher efficiencies in $Sb_2(S_{1-x}Se_x)_3$ solar cells.

In this work, the effect of loss mechanisms on antimony sulfide selenide cells is evaluated by an analytical model. A comparison between the model outcomes and the experimental data available in the literature is presented. In particular, the influence of defects at antimony sulfide selenide bulk and absorber /CdS interface is evaluated starting from representative parameters. The possible impact of tunneling mechanisms through defects on the device is also studied. Particularly, loss mechanisms are evaluated considering different compositions of the ternary compound. Finally, conditions that allow $Sb_2(S_{1-x}Se_x)_3$ device efficiencies larger than 14% are presented and discussed.

2 Model and parameter details

For solar cell parameters evaluation, the J-V characteristic is simulated for different compositions of the ternary compound and under each loss mechanism. The impact of each loss mechanism can be evaluated from the following equation [13]:

$$J = J_0\left[\exp\left(\frac{q(V - JR_S)}{2kT}\right) - 1\right] + \frac{V - JR_S}{R_{\mathrm{Sh}}} - J_{\mathrm{PH}} \tag{1}$$

where, J_{PH} is the photocurrent density, kT is the thermal energy, q is the electron charge and V is the applied voltage. In addition, R_{sh} and R_s are the shunt and series resistances, respectively. In Eq. (1), the reverse dark current density J_0 is a function of the assumed loss mechanism. It is observed in Eq. 1 that an ideality factor of 2 was considered for calculations. This consideration is mainly based on the experimental data reported for $Sb_2(SSe)_3$ solar cells [14]. In addition, loss mechanisms assumed for calculations are directly associated with the formation of defects, for which a diode ideality factor of 2 can be considered as a reasonable assumption [13]. In addition, the external quantum efficiency ($EQE_T(\lambda)$) of the device allows the evaluation of the photocurrent density, by considering the equation presented as follows:

$$J_{\mathrm{PH}} = q\int_{\lambda_1}^{\lambda_2} F(\lambda)\mathrm{EQE}_T(\lambda)\mathrm{d}\lambda \tag{2}$$

$F(\lambda)$ is the photon number obtained from the AM1.5G solar spectrum, in the range of 300–1300 nm. The superposition of EQE contributions from depletion zone ($EQE_{DZ}(\lambda)$) and n and p quasi-neutral zone ($EQE_N(\lambda)$, $EQE_P(\lambda)$) is considered to calculate EQE_T, as presented as follows:

$$\mathrm{EQE}_T(\lambda) = \mathrm{EQE}_P(\lambda) + \mathrm{EQE}_{N-\mathrm{CdS}}(\lambda) + \mathrm{EQE}_{N-\mathrm{ZnO}}(\lambda) + \mathrm{EQE}_{N-\mathrm{TCO}}(\lambda) + \mathrm{EQE}_{\mathrm{DZ}}(\lambda) \tag{3}$$

In particular, contributions of n and p quasi-neutral regions to EQE as a function of wavelength can be evaluated by the following equations [13]:

$$\mathrm{EQE}_P(\lambda) = \frac{\alpha_{\mathrm{Abs}}(\lambda)L_n[1 - R(\lambda)]\exp\{-\Sigma\alpha_i(\lambda)z_i\}}{\alpha_{\mathrm{Abs}}^2(\lambda)L_n^2 - 1} * \left\{\alpha_{\mathrm{Abs}}(\lambda)L_n - \frac{\frac{S_nL_n}{D_n}\left[\mathrm{Cosh}\left(\frac{d_{\mathrm{Abs}}}{L_n}\right) - \exp(-\alpha_{\mathrm{Abs}}(\lambda)d_{\mathrm{Abs}})\right] + \mathrm{Sinh}\left(\frac{d_{\mathrm{Abs}}}{L_n}\right) + \alpha_{\mathrm{Abs}}(\lambda)L_n\exp(-\alpha_{\mathrm{Abs}}(\lambda)d_{\mathrm{Abs}})}{\frac{S_nL_n}{D_n}\mathrm{Sinh}\left(\frac{d_{\mathrm{Abs}}}{L_n}\right) + \mathrm{Cosh}\left(\frac{d_{\mathrm{Abs}}}{L_n}\right)}\right\} \tag{4}$$

and

$$\mathrm{EQE}_N(\lambda) = \frac{\alpha_n(\lambda)L_p[1 - R(\lambda)]\exp\{-\Sigma\alpha_i(\lambda)z_i\}}{\alpha_n^2(\lambda)L_p^2 - 1} * \left\{\frac{\frac{S_pL_p}{D_p} + \alpha_n(\lambda)L_p - \exp(-\alpha_n(\lambda)d_n)\left[\frac{S_pL_p}{D_p}\mathrm{Cosh}\left(\frac{d_n}{L_p}\right) + \mathrm{Sinh}\left(\frac{d_n}{L_p}\right)\right]}{\frac{S_pL_p}{D_p}\mathrm{Sinh}\left(\frac{d_n}{L_p}\right) + \mathrm{Cosh}\left(\frac{d_n}{L_p}\right)} - \alpha_n(\lambda)L_p\exp(-\alpha_n(\lambda)d_n)\right\} \tag{5}$$

where L_p and L_n are minority carrier diffusion length values for n- and p-type materials, respectively. The terms $\alpha(\lambda)$ stand for the absorption coefficient of materials. Besides, the first exponential factor represents the photon attenuation in the front layers, which are described by the absorption coefficient $\alpha_i(\lambda)$ and thickness z_i. In addition, $R(\lambda)$ is the reflectivity spectrum of the surface, while S and D stand for recombination velocity at the surface and the diffusion coefficient of minority carriers, respectively. The n-type

and absorber quasi-neutral zone thicknesses are denoted by d_n and d_{Abs} terms, respectively. The contribution of depletion zone to EQE ($\mathrm{EQE}_{DZ}(\lambda)$) is evaluated by the following equation [13]:

$$\mathrm{EQE}_{\mathrm{DZ}}(\lambda) = [1 - R(\lambda)] \exp\{-\Sigma\alpha_i(\lambda) z_i\} \times \left[1 - \exp(-\alpha_{\mathrm{CdS}}(\lambda) x_{\mathrm{CdS}} - \alpha_{\mathrm{Abs}}(\lambda) x_{\mathrm{Abs}})\right] \tag{6}$$

where, x_{Abs} and x_{CdS} are depletion zone widths for absorber and CdS material, respectively. The absorption coefficient spectrum is required for EQE calculations. In particular, this parameter was calculated from the following equation for direct band-gap transitions [13]:

$$\alpha(E) = \frac{\sqrt{2} q^2 E_g \left[m_h^* * m_e^* / \left(m_h^* + m_e^*\right)\right]^{3/2}}{3\pi n c \varepsilon_0 m_e^* \hbar^2} * \frac{\sqrt{E - E_g}}{E} \tag{7}$$

where E_g is the band-gap of the analyzed semiconductor, and m_e^* and m_h^* are electron and hole effective masses, respectively. Besides, n is the refraction index, c is the speed of light, $\hbar$ is the reduced Planck constant, E is the energy of photons, q is the elemental charge of electron and ε_0 is the vacuum permittivity.

The Poisson's equation is considered to calculate the depletion zone characteristics such as electric field, potential barrier, and depletion width. On the other hand, in order to calculate the reflectivity between layers in the device, the Fresnel equations are considered [15].

2.1 Determination of J_0 term

The J_0 term can be calculated once defined the loss mechanism governing the device. Deep defects at absorber/buffer interface and bulk are often the cause of V_{oc} reduction in photovoltaics based on thin film materials. Therefore, this work aims at evaluating the impact of loss mechanisms favored by the deep defect formation, such as tunneling enhanced recombination as well as bulk and absorber/buffer interface recombination. That is, starting from typical values reported in the literature, the role of each loss mechanism can be evaluated, resulting in a better understanding of limiting factors concerning the $Sb_2(SSe)_3$/CdS solar cells. Details on each transport mechanism are presented in the following subsections.

2.1.1 Bulk recombination (SRH mechanism)

In $Sb_2(SSe)_3$ material, it has been observed that vacancies and substitutional defects might result in deep levels near the middle of the band-gap [8]. For CdS material, Cd vacancy defects are also expected near the middle of the material band-gap [16]. Therefore, the influence of defects at absorber and buffer layers on $Sb_2(SSe)_3$-based device performance is considered in this work. In particular, the Shockley–Read–Hall (SRH) theory is used for the evaluation of recombination losses. The impact of bulk defects on reverse saturation current density can be evaluated by the following equation [13]:

$$J_{0-\mathrm{SRH}} = q\left(\frac{x_n n_{i-\mathrm{CdS}}}{\tau_n} + \frac{x_p n_{i-\mathrm{SbSSe}}}{\tau_p}\right) \tag{8}$$

where, τ is the minority carrier lifetime, which depends on defect properties. In this work, typical values experimentally reported for minority carrier lifetimes are considered for calculations.

2.1.2 Tunneling enhanced recombination

In p-n junctions, the presence of an electric field at the depletion layer may favor the increase in recombination by a tunneling process through shallow defects. Recombination enhanced by the presence of the tunneling of carriers is often called tunneling enhanced recombination, which has been identified as dominant in other technology such as kesterite [17, 18]. In $Sb_2(SSe)_3$ and CdS materials, shallow states contributing to the p-type and n-type conductivities, respectively, could favor the recombination process [8, 16]. The contribution of the tunneling mechanism to carrier recombination was proposed by Hurkx et al., starting from the SRH theory [11, 19]. Taking into account the proposal of Hurkx, the reverse dark current density under this mechanism is given by [13]:

$$J_{0-\mathrm{TER}} = q\left(\frac{x_n n_{i-\mathrm{CdS}}(1 + \Gamma_{\mathrm{CdS}})}{\tau_n} + \frac{x_p n_{i-\mathrm{SbSSe}}(1 + \Gamma_{\mathrm{SbSSe}})}{\tau_p}\right) \tag{9}$$

where Γ stands for the effect of carrier tunneling. Under a weak electric field, the model reduces to the conventional SRH equation (Eq. 8).

2.1.3 *CdS/$Sb_2(SSe)_3$ interface recombination*

Heterojunction solar cells are often described with a high interfacial defect formation as a result of the different lattice constants and structures of materials. The interface recombination has been identified as dominant in other technology such as kesterite [18]. It has been previously shown that J_0 under the interface recombination can be calculated by equation [13]:

$$J_{0-\mathrm{IR}} = q\mathrm{Sn}_{i-\mathrm{SbSSe}}\left(1+\gamma_{\mathrm{DOS}}e^{-(\Delta E_C+\Delta E_V)/2kT}\right) \tag{10}$$

where ΔE_c and ΔE_v are the conduction and valence band offsets, respectively. In addition, S is the absorber/buffer interface recombination speed and γ_{DOS} is the ratio of CdS to $Sb_2(S,Se)_3$ effective densities of states.

In general, Eqs. (1–10) allow the evaluation of current density–voltage characteristics of $Sb_2(S,Se)_3$ solar cells dominated by each loss mechanism. After this, the optoelectronic device parameters behavior under different conditions can be assessed.

2.2 Model parameters and software details

In order to verify the model, a Sb_2Se_3 solar cell with Mo/Sb_2Se_3/CdS/In_2O_3:Sn structure was simulated in the first calculations, and compared with a typical device reported in the literature [20]. Since the use of In_2O_3:Sn (ITO) in solar cells can result in a higher cost of the device due to the low abundant In element, for further calculations, we considered the use of the traditional ZnO:Al as transparent conducting oxide (TCO). In this sense, after the validation of the model, ITO is replaced by ZnO:Al (AZO) and an intrinsic buffer layer of ZnO is used between the CdS and AZO as reported in traditional thin film solar cells with substrate configuration. In addition, Sb_2Se_3 absorber is replaced with $Sb_2(S,Se)_3$ in solar cells to study the effect of different compositions of the ternary compound. That is, solar cells with glass/Au/$Sb_2(SSe)_3$/CdS/ZnO/ZnO:Al configuration are considered for the next calculations. The In_2O_3:Sn (ITO), ZnO:Al (AZO), ZnO and CdS properties used for simulations are shown in Table 1. These values based on experimental and theoretical reports have been previously used for devices modeling [21]. So far, most properties of the ternary material as functions of composition are unknown. On the other hand, since Sb_2S_3 and Sb_2Se_3 materials have been intensively studied, their properties are available in the literature. Consequently, a linear variation with composition for $Sb_2(S,Se)_3$ properties is assumed, between those of the binaries for simplicity. Typical values of Sb_2S_3 and Sb_2Se_3 material properties considered for calculations of $Sb_2(S,Se)_3$ solar cells are presented in Table 2. Furthermore, an electron affinity of 3.98 eV for CdS material has been considered for calculation as published before [29]. Carrier lifetime values in the order of nanoseconds have been measured for $Sb_2(S,Se)_3$ material [30, 31]. In this sense, a carrier lifetime value of 5 ns is firstly considered for simulations and later changed. From effective masses presented in Table 2, the effective density of states of bands can be calculated. In addition, mobility values allow finding diffusion coefficient and diffusion length values of minority carriers. For the accurate reproduction of Sb_2Se_3 solar cell experimental data, it was necessary to use a low Sb_2Se_3/CdS interface recombination speed value of 1×10^4 cm/s, which was estimated from typical values of thermal velocity and carrier cross section considering that authors estimated an interface density of defects of 1×10^{11} cm^{-2} [20]. For the next calculations of the ternary-based solar cell, we consider that it is better to use a typical recombination speed value of 4×10^4 cm/s at $Sb_2(SSe)_3$/CdS interface in the first calculations in order not to underestimate the interface losses. This value allows the reproduction of the experimental data reported for $Sb_2(SSe)_3$ solar cells. In a subsequent analysis, the interface recombination speed was changed in the range of 1–10^5 cm/s for a better estimation of the role of this mechanism. On the other hand, typical front

Table 1 Simulation parameters for In_2O_3:Sn (ITO), ZnO:Al (AZO), ZnO, and CdS films

Parameters	In_2O_3:Sn (ITO)	ZnO:Al (AZO)	ZnO	CdS
Relative dielectric permittivity (ε_r)	2	9	9	9
Hole mobility, μ_p (cm^2/V s)	75	25	25	50
Donor concentration, N_D (cm^{-3})	10^{20}	10^{20}	10^{18}	10^{17}
Band Gap (eV)	3.6	3.3	3.3	2.4
Conduction band effective density of states, N_c (cm^{-3})	2×10^{20}	2.2×10^{18}	2.2×10^{18}	1.8×10^{19}
Valence band effective density of states, N_v (cm^{-3})	1.8×10^{19}	1.8×10^{19}	1.8×10^{19}	2.4×10^{18}
Defect density(cm^{-3})	10^{17}	10^{17}	10^{17}	10^{17}
Hole capture cross section (cm^2)	10^{-15}	10^{-15}	10^{-15}	10^{-13}
Hole thermal velocity (m/s)	10^7	10^7	10^7	10^7
Electron effective mass, m_e^*/m_0	0.3	0.275	0.275	0.25
Hole effective mass, m_h^*/m_0	0.6	0.59	0.59	0.7
Thickness (nm)	500	500	30	100

Table 2 Parameters of binary compounds used for the estimation of $Sb_2(S,Se)_3$ properties

Parameters	Sb_2S_3	Sb_2Se_3	References
Electron affinity (eV)	3.7	4.04	[13, 22]
Band-gap (eV)	1.62	1.08	[5]
Dielectric constant	22	15.1	[23]
Carrier mobility (cm^2/Vs)	9.8	21.88	[7, 24]
Electron effective mass	1.035 m_0	0.365m_0	[25, 26]
Hole effective mass	1.843 m_0	0.316m_0	[25, 26]
Refractive index	3.4	4.4	[27]
Aceptor concentration (cm^{-3})	10^{12}	10^{15}	[7, 28]
Thickness (μm)	1.3	1.3	

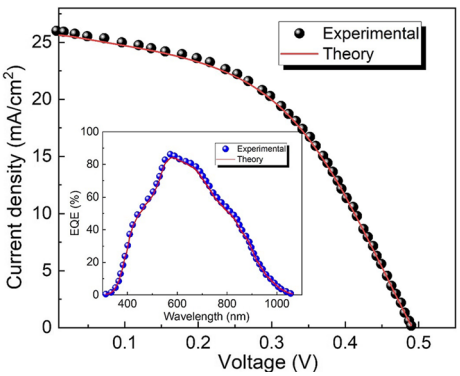


Fig. 1 Comparison between the experimental data and model results for external quantum efficiency (inset) and J-V characteristics of a typical Sb_2Se_3 solar cell

and back surface recombination velocity values of 10^5 cm/s for minority carriers were taken into account [13]. For calculations, measured values of 57 Ωcm^2 and 701 Ωcm^2 for series and shunt resistances, respectively, [20] were initially considered for the validation of Sb_2Se_3 solar cell simulation and later changed to typical values of 6.1 Ωcm^2 and 290.5 Ωcm^2, respectively, reported for $Sb_2(SSe)_3$ solar cells [32]. For calculating the surface reflectivity and $EQE_T(\lambda)$ spectra, extinction coefficient and the refractive index of ZnO [33, 34] and CdS [35] were considered. The extinction coefficient of $Sb_2(S,Se)_3$ compound is evaluated from the absorption coefficient and the refractive index reported in reference [27]. The AM 1.5G data characterized by a power density of 100 mW/cm^2 were used to evaluate the optoelectronic parameters.

Wolfram Mathematica version 6.0 was used to elaborate a package for solar cell modeling. Other solar cell technologies have been simulated by this package [9, 13, 17, 18]. All transport equations and constants are available in the package. The current–voltage characteristics (J-V) and external quantum efficiency (EQE) of solar cells can be simulated for the different loss mechanisms and input parameters. Once known the J-V characteristics, the optoelectronic parameters are numerically calculated. The J_0 (Eq. 8–10) and J_{PH} (Eq. 2) are firstly calculated for the evaluation of J-V characteristics. The superposition of J_0 values corresponding to each mechanism is assumed under the effect of the simultaneous contribution of mechanisms. Therefore, the role of input parameters on solar cell behavior can be evaluated for each mechanism and their simultaneous contribution.

3 Results and discussion

Before performing calculations on the influence of mechanisms on solar cells, the validation of the model is an important first step. For this purpose, a typical solar cell with Mo/Sb_2Se_3/CdS/In_2O_3:Sn configuration with an efficiency of 6.06% was considered for comparison as reported in the literature [20]. The simultaneous influence of defects at Sb_2Se_3 bulk and CdS/Sb_2Se_3 interface was considered in order to reproduce the experimental data. The comparison between simulation results and the experimental data is presented in Fig. 1 for J-V and EQE characteristics. A good agreement between the simulation results and the experimental data is observed. This fact is confirmed by the comparison between experimental and theoretical results of the optoelectronic parameters as presented in Table 3. It is observed that the good match of theoretical EQE to the experimental data allows obtaining a short-circuit current density near the one measured for the device. A maximum EQE of 86% illustrated in Fig. 1 indicates that about 14% of incident photons with energy between Sb_2Se_3 band-gap and CdS band-gap are lost. This result could be associated with shading and photon reflection losses along with a low diffusion length due to the presence of bulk defects. In this work, we have only considered losses due to photon reflection and low diffusion length to reproduce the experimental data. Therefore, these points are open research for this technology. On the other hand, it is pointed out that under the simultaneous effect of loss mechanisms, the open-circuit voltage of the device was reproduced starting from typical parameter values. In addition, a low fill factor value is

Table 3 Comparison between experimental data and the model results for Sb_2Se_3 solar cells

Parameter	Efficiency (%)	FF (%)	J_{sc} (mA/cm^2)	V_{oc} (V)
Model results	6.11	48.12	25.6	0.496
Experimental [20]	6.06	47.73	25.91	0.494

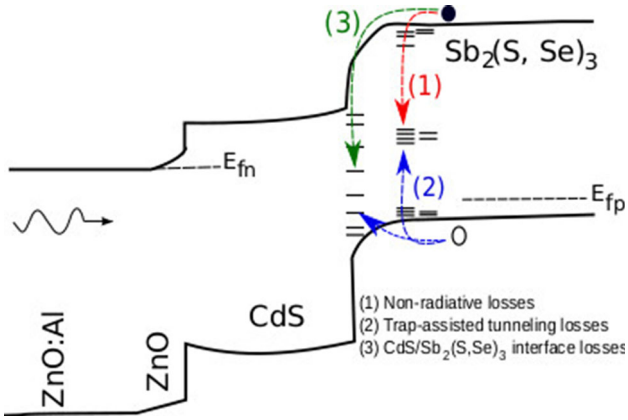


Fig. 2 Sketch of ZnO:Al/ZnO/CdS/$Sb_2(SSe)_3$ solar cell. Recombination mechanisms such as bulk (non-radiative recombination or SRH), trap-assisted tunneling recombination (tunneling enhanced recombination) and $Sb_2(SSe)_3$/CdS interface recombination are presented

Table 4 Efficiency, fill factor, short-circuit current density (J_{sc}) and open-circuit voltage (V_{oc}) of $Sb_2(S_{0.6}Se_{0.4})_3$ solar cells under $Sb_2(S_{0.6}Se_{0.4})_3$/CdS interface recombination (Int), $Sb_2(S_{0.6}Se_{0.4})_3$ bulk recombination (SRH), tunneling enhanced recombination (TER) and their simultaneous contribution

Loss mechanism	Efficiency (%)	FF(%)	J_{sc}(mA/cm^2)	V_{oc}(V)
Int	6.9	52.9	21.72	0.601
SRH	6.38	51.6	21.72	0.569
TER	6.25	51.3	21.71	0.561
Int-SRH	6.02	50.7	21.71	0.547
Int-TER	5.93	50.4	21.71	0.542

expected from the simulations, which is also very close to the experimental reported one. As a result, an efficiency value in good correspondence to the experimental data is found. It should be noted that Fig. 1 and Table 3 showed not only the reproduction of the experimental optoelectronic parameters but also the shape of J-V and EQE curves with acceptable differences. Therefore, the model and parameters assumed for calculations were able to accurately reproduce the experimental data and thereby further estimations can be performed.

For the next calculations, the ITO is replaced by AZO to reduce the cost of the device for the low abundance of In element. A typical ZnO intrinsic buffer layer is used between AZO and CdS as published elsewhere for thin film solar cells with substrate configuration. In addition, S element is introduced into the Sb_2Se_3 material to form the $Sb_2(S,Se)_3$ ternary compound. The impact of bulk defects (SRH recombination)—also known as non-radiative losses –, tunneling enhanced recombination (TER)—also known as trap-assisted tunneling losses –, defects at $Sb_2(SSe)_3$/CdS interface (Interface recombination) and their simultaneous contribution on antimony sulfide selenide solar cells is taken into account for further calculations. Figure 2 illustrates the effect of each mechanism in carrier losses. In particular, a Se concentration of 0.4 was initially considered, for which an optimized solar cell efficiency of about 29% was obtained in a previous work under ideal conditions [9]. The J-V characteristics of $Sb_2(S_{0.6}Se_{0.4})_3$ under the impact of different loss mechanisms are shown in Fig. 3, while the optoelectronic parameters are presented in Table 4. In comparison with the previous results of reference [9], where calculations are performed under the radiative limit, it is demonstrated that loss mechanisms due to defects can reduce device efficiency to values as published elsewhere for antimony sulfide selenide solar cells with p-n configuration (<7%). Among all the optoelectronic parameters, it is illustrated that reduced V_{oc} remains as one important drawback. In particular, V_{oc} values in the range of 542–601 mV are expected depending on the loss mechanism considered in the calculation. That is, only a V_{oc} variation near to 60 mV is obtained between mechanisms for typical values assumed for calculation. Therefore, it is demonstrated that both interface and bulk defects play a dominant role in device behavior. The comparison between Tables 3 and 4 demonstrates that the incorporation of S into the lattice of Sb_2Se_3 material results in the reduction of J_{sc} and the promotion of V_{oc} due to the increase in band-gap with the partial replacement of Se by S atoms. Furthermore, the reduction in series resistance and the increase in shunt resistance in $Sb_2(S_{0.6}Se_{0.4})_3$ solar cells in comparison to Sb_2Se_3 solar cells result in the increase in fill factor.

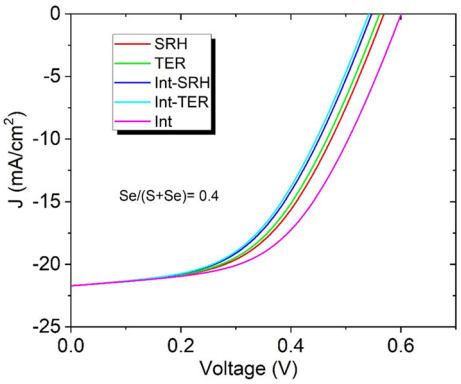


Fig. 3 Current density–voltage curves of $Sb_2(SSe)_3$ solar cells under bulk recombination (SRH), tunneling enhanced recombination (TER), $Sb_2(SSe)_3$/CdS interface recombination and their simultaneous contribution for a Se composition of 0.4

In the next step, the impact of all mechanisms under different Se compositions on device parameters is calculated. The optoelectronic parameters behavior with composition under each mechanism is illustrated in Fig. 4. Figure 4a shows $Sb_2(S, Se)_3$ solar cell efficiency dependence on Se composition. A slight efficiency enlargement with Se composition increasing until a value of about 0.2 is found for all loss mechanisms. On the contrary, efficiency is reduced for all loss mechanisms considered for calculations when Se composition is higher than 0.2. This trend is the direct result of the trade-off between the increase of J_{sc} and the reduction of V_{oc} with Se composition increasing as illustrated in Fig. 4b, c, respectively. In this sense, these results point out that under current experimental conditions in which $Sb_2(SSe)_3$/CdS solar cells are fabricated, Se compositions lower than 0.3 are better for achieving the highest solar cell efficiencies. However, low efficiency values in the range of 6.5–7.5% would be obtained. This result demonstrates that the Se composition variation is not an effective route to promote solar cell performance under the dominant effect of defects at bulk and interface. It is also observed in Fig. 4a that there is no significant variation in solar cell efficiency from one mechanism to another. Figure 4b illustrates that short-circuit current density values ranging 14–30 mA/cm^2 are expected. In particular, J_{sc} is increased with the increase of Se composition due to the band-gap decrease. It should be noted for the sake of clarity that higher J_{sc} values are found for Sb_2Se_3 solar cells (ternary with Se composition equals 1) in Fig. 4b in comparison to the value obtained in Table 3 since a lower series resistance was adopted for the ternary-based solar cell calculations as mentioned in the parameter details section. Figure 4c shows the V_{oc} dependence on Se composition for each loss mechanism. A V_{oc} reduction with Se composition increase is found, which can be explained by taking into account the increase in reverse dark current density with Se composition (Fig. 4d). A V_{oc} variation among all loss mechanisms of about 50 mV is illustrated, which is a result of the reverse dark current density variation lower than an order of magnitude as presented in Fig. 4d. Consequently, the effect of bulk and interface defects should be considered for further analyses. A V_{oc} variation from 0.8 to 0.3 V is obtained with Se composition enlarging from 0 to 1, due to the band-gap decrease. For the sake of clarity, it is also pointed out that lower V_{oc} values are found for Sb_2Se_3 solar cells (ternary with Se composition equals 1) in Fig. 4c in comparison to the value obtained in Table 3 since a higher Sb_2Se_3/CdS interface recombination speed was adopted for the ternary-based solar cell calculations as mentioned in the parameter details section. Since TER entails SRH recombination, which is enlarged with the assistance of the built-in potential of the junction—under a negligible effect of the electric field, TER turns into SRH –, further calculations are performed under the simultaneous contribution of TER and $Sb_2(SSe)_3$/CdS interface recombination.

The formation of bulk defects has a direct impact on carrier lifetime. The influence of $Sb_2(SSe)_3$ carrier lifetime on the optoelectronic parameters was taken into account in a further step. A selenium composition of 0.2 was considered based on results presented in Fig. 4a. In addition, the role of carrier lifetimes ranging from 0.1 ns to 1 ms is evaluated. A value of 0.1 ns is associated with an absorber material with poor crystallinity, while values near 1 ms consider the case of an absorber with a negligible contribution of defects. The dependence of efficiency, J_{sc}, V_{oc} and FF on $Sb_2(S_{0.8}Se_{0.2})_3$ minority carrier lifetime is presented in Fig. 5. An efficiency promotion from 4 to 7.2% can be obtained for carrier lifetime increasing from 0.1 ns to 10^{-7} s. However, efficiency does not change for minority carrier lifetime higher than 10^{-7} s, which accounts for the dominant role of losses at $Sb_2(SSe)_3$/CdS interface, limiting the further promotion of the device efficiency. Therefore, it is demonstrated that current $Sb_2(SSe)_3$/CdS devices are not only limited by $Sb_2(SSe)_3$ bulk defects. In fact, if $Sb_2(SSe)_3$ bulk defects were the only loss mechanism, efficiencies higher than 7% would be expected under good crystalline quality. This means that the reduction in bulk defects is not the unique solution to achieving higher solar cell efficiency. Figure 5b shows a J_{sc} variation lower than 1 mA/cm^2 with carrier lifetime increase. In contrast, significant V_{oc} promotion of about 220 mV can be obtained for a higher carrier lifetime. However, V_{oc} does not overcome the value of 700 mV. Fill factor values are also lower than 60%, emphasizing the need for ideal resistances.

$Sb_2(SSe)_3$/CdS interface defect influence on the solar cell is evaluated in the next step. The impact of values ranging 1–10^5 cm/s on efficiency and V_{oc} is shown in Fig. 6a, b, respectively. In particular, calculations are performed for the case of non-optimized minority carrier lifetime (5 ns) and optimized minority carrier lifetime with almost an ideal value (10^{-5} s), for comparison. It is pointed out that for a non-optimized minority carrier lifetime, an efficiency enhancement lower than 1% is found with the reduction in interface defects, due to a low V_{oc} increase lower than 100 mV as shown in Fig. 6b. This result demonstrates that the reduction

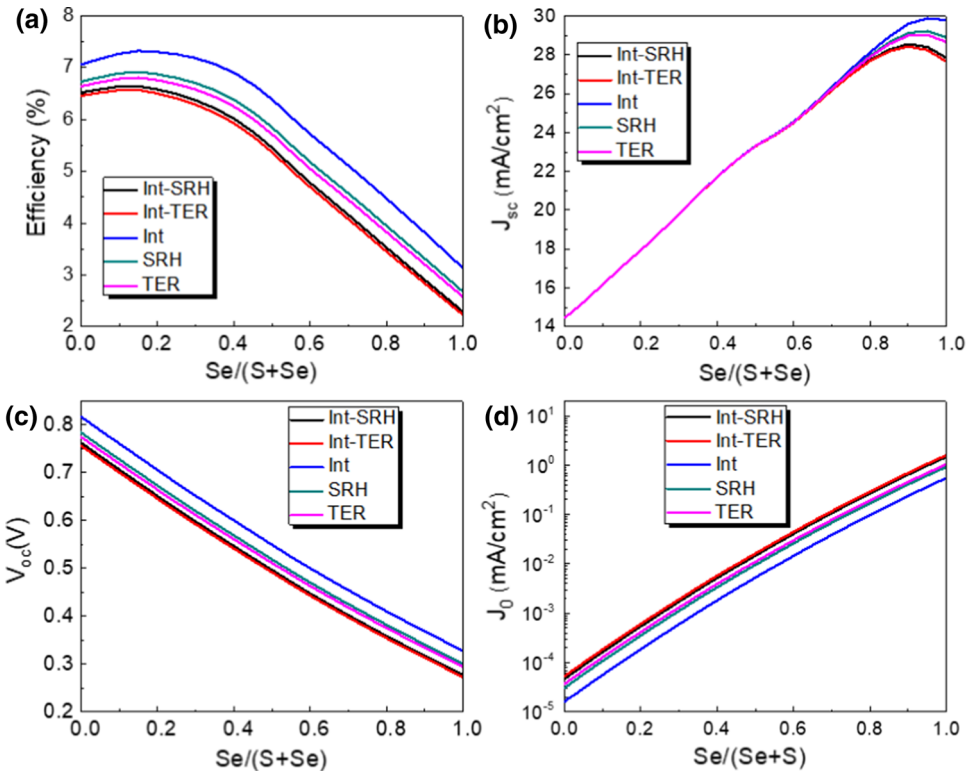


Fig. 4 Dependence of efficiency (**a**), short-circuit current density (**b**), open-circuit voltage (**c**) and reverse dark current density (J_0) (**d**) on Se composition for the different loss mechanisms

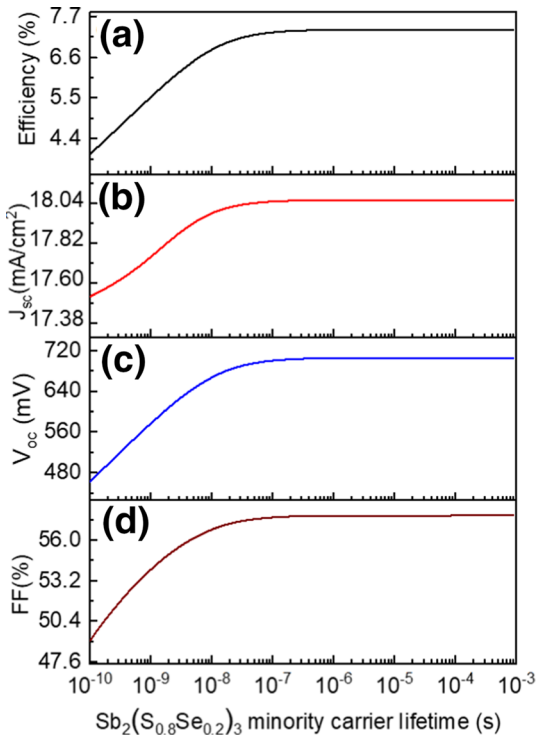


Fig. 5 Influence of absorber minority carrier lifetime on efficiency (**a**), short-circuit current density (**b**), open-circuit voltage (**c**) and fill factor (FF) (**d**) for a Se composition of 0.2

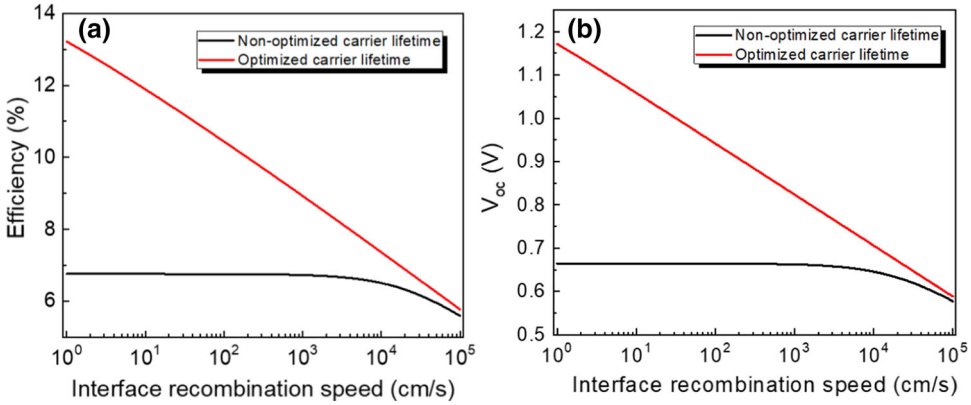


Fig. 6 Impact of interface recombination speed on efficiency (**a**) and open-circuit voltage (**b**) for an optimized and non-optimized minority carrier lifetime

in interface recombination speed is not by itself the solution for achieving efficiencies higher than 7%. It is interesting to note that when comparing the results of Figs. 5a and 6a, a higher impact on solar cell efficiency is expected from the minority carrier lifetime variation. In this sense, for typical values assumed for calculations, bulk and interface defects are presented as the main limiting factors concerning this technology. For an optimized carrier lifetime with almost an ideal value (10^{-5} s), a remarkable efficiency improvement to values about 13% is observed with the reduction in interface defects, due to a V_{oc} promotion to 1.15 V as illustrated in Fig. 6a, b. Therefore, this result highlights the need for reducing the effect of bulk defects and interface defects. Otherwise, an efficiency higher than 8% could be not reached.

The impact of different values of absorber/buffer interface recombination speed and absorber minority carrier lifetime on efficiency and V_{oc} is shown in Fig. 7, under the effect of series and shunt resistances ((a) and (b)) and under the consideration of ideal series and shunt resistances ((c) and (d)). A general trend is observed, where efficiency and V_{oc} are independent of the interface recombination speed for very low minority carrier lifetime values in the order of 0.1 ns. For minority carrier lifetime values higher than 1 ns, the effect of both bulk and interface defects is dominant. For very low interface recombination speed values and very high minority carrier lifetime values, an efficiency near 16.2% with an open-circuit voltage of 1.18 V could be obtained. Therefore, a maximum efficiency of 16% is expected in this type of solar cell under optimized minority carrier lifetime and interface recombination speed values. The comparison between results with and without resistances demonstrates that resistances present a negligible impact on V_{oc}. On the contrary, under ideal resistances, a solar cell efficiency of 21.8% is expected for a Se composition of 0.2, when a minority carrier lifetime of 1 ms and an interface recombination speed of 1 cm/s are assumed.

Finally, the dependence of each loss mechanism on Se composition is evaluated under optimized conditions for bulk (100 ns) and interface (1 cm/s); results are presented in Fig. 8. Calculations were performed without series and shunt resistances. Under a negligible effect of interface defects, efficiencies in the range of 17–18% could be reached for Se compositions bigger than 0.5. On the other hand, a maximum efficiency of about 14.5% is expected under a surface recombination speed of 1 cm/s for Se compositions bigger than 0.4. In addition, results illustrate that there is an overlapping of curves corresponding to IR, IR + SRH and IR + TER, demonstrating the dominant role of interface defects. Therefore, this result demonstrates that efficiencies bigger than 14.5% can be only obtained for recombination speed values shorter than 1 cm/s. In fact, Fig. 8 demonstrates that interface defect decrease results in an efficiency promotion from 14.5 to 17.5%. Another important feature from Fig. 8 is that the choice of the optimal Se composition depends on the loss mechanism limiting the device. That is, under the dominance of interface recombination (for 1 cm/s), an optimal Se composition near to 0.5 is found, while under a negligible impact of $Sb_2(SSe)_3$/CdS interface defects, an optimal Se composition of about 0.9 is obtained (for 100 ns). In this work, all calculations demonstrate that TER mechanism results in optoelectronic parameters that are near to the ones of SRH mechanism. As a result, the electric field at the heterojunction is not playing a dominant role. In this sense, SRH mechanism can be used to understand the main limitations of this technology.

4 Conclusions

In short, we have presented results concerning a theoretical study on the impact of $Sb_2(S_{1-x}Se_x)_3$ bulk recombination, tunneling enhanced recombination and $Sb_2(S_{1-x}Se_x)_3$/CdS interface recombination on optoelectronic parameters of the device for different Se compositions, for the first time. It was demonstrated that for typical parameters chosen for simulations, bulk and interface recombinations constitute the main problems that degrade the device performance. In addition, we found that the tunneling enhanced recombination mechanism can be neglected in comparison to SRH mechanism in calculations; in this sense SRH theory is an adequate approach to evaluate the effect of bulk defects. The reduction in the impact of both interface and bulk defects was introduced as mandatory for efficiency promotion. We found that experimentalists working on either the reduction in defects at interface or defects at bulk would not be able to obtain efficiencies bigger than 10%. On the contrary, under a carrier lifetime higher than 100 ns and an

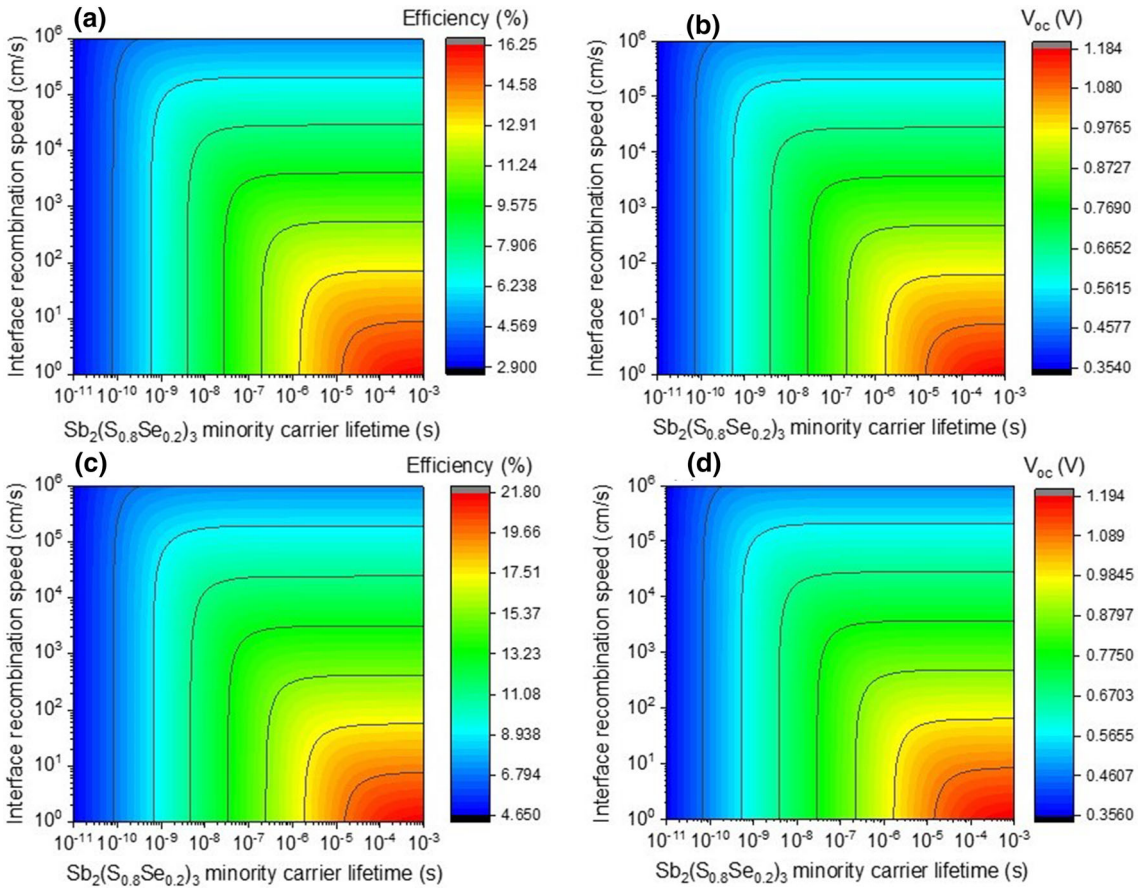


Fig. 7 Impact of interface recombination speed and absorber minority carrier lifetime on efficiency and open-circuit voltage of the solar cell, considering the effect of series and shunt resistances ((**a**) and (**b**)) and without the effect of series and shunt resistances ((**c**) and (**d**))

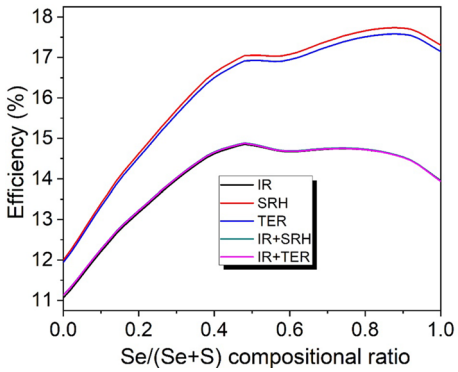


Fig. 8 Influence of each loss mechanism and Se composition on efficiency for optimized values of interface recombination and bulk minority carrier lifetime without the effect of resistances

interface recombination speed lower than 1 cm/s, efficiencies higher than 14% are expected. Therefore, further experimental studies should be focused on the reduction in recombination at $Sb_2(S_{1-x}Se_x)_3$ bulk and $Sb_2(S_{1-x}Se_x)_3$/CdS interface.

Acknowledgements M. Courel thanks support from pro-SNI of University of Guadalajara. T. Jimenez acknowledges fellowship support from CONACyT for master degree study. LMP and DL acknowledge partial financial support from FONDECYT 1180905. DL acknowledges partial financial support from Centers of excellence with BASAL/CONICYT financing, AFB 180001, CEDENNA. LMP acknowledges financial support from ANID through Convocatoria Nacional Subvención a Instalación en la Academia Convocatoria Año 2021, Grant SA77210040.

Data availability This manuscript has associated data in a data repository. [Authors' comment: The data that support the findings of this study are available from the corresponding author upon reasonable request.]

References

1. M. Green, E. Dunlop, J. Hohl-Ebinger, M. Yoshita, N. Kopidakis, X. Hao, Prog. Photovolta. Res. Appl. **29**, 3–15 (2021). https://doi.org/10.1002/pip.3371
2. S. Lu, Y. Zhao, X. Wen, D.-J. Xue, C. Chen, K. Li, R. Kondrotas, C. Wang, J. Tang, Sol. RRL **3**, 1800280 (2019). https://doi.org/10.1002/solr.201800280
3. H. Lei, J. Chen, Z. Tan, G. Fang, Sol. RRL **3**, 1900026 (2019). https://doi.org/10.1002/solr.201900026
4. R. Tang, X. Wang, W. Lian, J. Huang, Q. Wei, M. Huang, Y. Yin, C. Jiang, S. Yang, G. Xing, S. Chen, C. Zhu, X. Hao, M.A. Green, T. Chen, Nat. Energy **5**, 587–595 (2020). https://doi.org/10.1038/s41560-020-0652-3
5. B. Yang, D.J. Xue, M. Leng, J. Zhong, L. Wang, H. Song, Y. Zhou, J. Tang, Nat. Sci. Rep. **5**, 10978 (2015). https://doi.org/10.1038/srep10978
6. O. Vigil-Galán, M. Espíndola-Rodríguez, M. Courel, X. Fontané, D. Sylla, V. Izquierdo-Roca, A. Fairbrother, E. Saucedo, A. Pérez-Rodríguez, Sol. Energy Mater. Sol. Cells **117**, 246–250 (2013). https://doi.org/10.1016/j.solmat.2013.06.008
7. X. Wang, R. Tang, C. Wu, C. Zhu, T. Chen, J. Energy Chem. **27**, 713–721 (2017). https://doi.org/10.1016/j.jechem.2017.09.031
8. J. Dong, Y. Liu, Z. Wang, Y. Zhang. Nano Select. **2**(10), 1818–1848 (2021). https://doi.org/10.1002/nano.202000288
9. T. Jiménez, D. Seuret-Jiménez, O. Vigil-Galán, M.A. Basurto-Pensado, M. Courel, J. Phys. D: Appl. Phys. **51**, 435501 (2018). https://doi.org/10.1088/1361-6463/aaddea
10. A. Haddout, M. Fahoume, A. Qachaou, A. Raidou, M. Lharch, Sol. Energy **211**, 301–311 (2020). https://doi.org/10.1016/j.solener.2020.09.067
11. G.A.M. Hurkx, D.B.M. Klassen, M.P.G. Knuvers, IEEE Trans. Electron Devices **39**, 331 (1992). https://doi.org/10.1109/16.121690
12. J. Tao, X. Hu, J. Xue, Y. Wang, G. Weng, S. Chen, Z. Zhu, J. Chu, Sol. Energy Mater. Sol. Cells **197**, 1–6 (2019). https://doi.org/10.1016/j.solmat.2019.04.003
13. M. Courel, T. Jiménez, A. Arce-Plaza, D. Seuret-Jiménez, J.P. Morán-Lázaro, F.J. Sánchez-Rodríguez, Sol. Energy Mater. Sol. Cells **201**, 110123 (2019). https://doi.org/10.1016/j.solmat.2019.110123
14. X. Wang, R. Tang, C. Jiang, W. Lian, H. Ju, G. Jiang et al., Adv. Energy Mater. **10**, 2002341 (2020). https://doi.org/10.1002/aenm.202002341
15. M. Born, E. Wolf, *Principles of Optics*, 4th edn. (Pergamon Press, Oxford, 1970)
16. J.B. Varley, V. Lordi, Appl. Phys. Lett. **103**, 102103 (2013). https://doi.org/10.1063/1.4819492
17. M. Courel, E. Valencia-Resendiz, J.A. Andrade-Arvizu, E. Saucedo, O. Vigil-Galán, Sol. Energy Mater. Sol. Cells **159**, 151–158 (2017). https://doi.org/10.1016/j.solmat.2016.09.004
18. M. Courel, J.A. Andrade-Arvizu, O. Vigil-Galán, Mater. Res. Express **3**, 095501 (2016). https://doi.org/10.1088/2053-1591/3/9/095501
19. G.A.M. Hurkx, H.C. de Graaff, W.J. Kloosterman, M.P.G. Knuvers, IEEE Trans. Electron Devices **39**, 2090–2098 (1992). https://doi.org/10.1109/16.155882
20. Z.-H. RongTang, Su. Zheng-Hua, X.-J. Li, Y.-D. Wei, X.-H. Zhang, Fu. Yong-Qing, J.-T. Luo, P. Fan, G.-X. Liang, Nano Energy **64**, 103929 (2019). https://doi.org/10.1016/j.nanoen.2019.103929
21. M. Courel, O. Vigil-Galan, *Different approaches for thin film solar cell simulation book: advanced ceramic and metallic coating and thin film materials for energy and environmental applications* (Springer, Berlin, 2018)
22. Yu. Cao, C. Liu, J. Jiang, X. Zhu, J. Zhou, J. Ni, J. Zhang, J. Pang, M.H. Rummeli, W. Zhou, H. Liu, G. Cuniberti, Sol. RRL **5**, 2000800 (2021). https://doi.org/10.1002/solr.202000800
23. O. Madelung, *Semiconductors: Data Handbook* (Springer-Verlag, Berlin Heidelberg, 2004). https://doi.org/10.1007/978-3-642-18865-7
24. C. Yuan, L. Zhang, W. Liu, C. Zhu, Sol. Energy **137**, 256 (2016). https://doi.org/10.1016/j.solener.2016.08.020
25. A. Stoliaroff, A. Lecomte, O. Rubel, S. Jobic, X. Zhang, C. Latouche, X. Rocquefelte, A.C.S. Appl, Energy Mater. **3**, 2496 (2020). https://doi.org/10.1021/acsaem.9b02192
26. L.I. Validzic, M. Mitric, N.D. Abazovic, B.M. Jokic, A.S. Milosevic, Z.S. Popovic, F.R. Vukajlovic, Semicond. Sci. Technol. **29**, 035007 (2014)
27. E.A. El-Sayad, J. Non-Cryst, Solids **354**, 3806–3811 (2008). https://doi.org/10.1016/j.jnoncrysol.2008.05.004
28. X. Liu, X. Xiao, Y. Yang, D.J. Xue, D.B. Li, C. Chen, S. Lu, L. Gao, Y. He, M.C. Beard, G. Wang, S. Chen, J. Tang, Prog. Photovolt. Res. Appl. **25**, 861–870 (2017). https://doi.org/10.1002/pip.2900
29. S. Yuan, H. Deng, D. Dong, X. Yang, K. Qiao, C. Hu, H. Song, H. Song, Z. He, J. Tang, Sol. Energy Mater. Sol. Cells **157**, 887–93 (2016). https://doi.org/10.1016/j.solmat.2016.07.050
30. X. Chen, Z. Li, H. Zhu, Y. Wang, B. Liang, J. Chen, Y. Xu, Y. Mai, J. Mater. Chem. C **5**, 9421–9428 (2017). https://doi.org/10.1039/C7TC02460F
31. H. Deng, S. Yuan, X. Yang, J. Zhang, J. Khan, Y. Zhao et al., Prog. Photovolt. Res. Appl. **26**, 281–290 (2018). https://doi.org/10.1002/pip.2980
32. Y. Zhang, J. Li, G. Jiang, W. Liu, S. Yang, C. Zhu, T. Chen, Sol. RRL **1**, 1700017 (2017). https://doi.org/10.1002/solr.201700017
33. W.N. Shafarman, S. Siebentritt, L. Stolt, *Handbook of Photovoltaic Science and Engineering*, 2nd edn. (John Wiley & Sons Ltd, West Sussex, UK, 2011), pp. 546–599
34. Z.-H. Dai, R.-J. Zhang, J. Shao, Y.-M. Chen, Y.-X. Zheng, J.-D. Wu, L.-Y. Chen, Optical properties of zinc-oxide films determined using spectroscopic ellipsometry with various dispersion models. J. Korean Phys. Soc. **55**, 1227–1232 (2009). https://doi.org/10.3938/jkps.55.1227
35. S. Ninomiya, S. Adachi, J. Appl. Phys. **78**, 1183–1190 (1995). https://doi.org/10.1063/1.360355